

Chemical effects on the $K\beta''$ and $K\beta_{2,5}$ x-ray lines of titanium and its compounds

Luka Mandić*

Physics Department, University of Rijeka, Omladinska 14, HR-51000 Rijeka, Croatia

Stjepko Fazinić and Milko Jakšić

Rudjer Bošković Institute, Bijenička cesta 54, HR-10000 Zagreb, Croatia

(Received 1 June 2009; published 30 October 2009)

High-resolution $K\beta$ x-ray spectra induced by 2 MeV protons in thick Ti, TiO, Ti₂O₃, TiO₂, MgTiO₃, FeTiO₃, TiC, TiN, and TiB₂ targets were measured using a wavelength dispersive spectrometer combined with a position-sensitive detector. The intensities and energies of the $K\beta_{2,5}$ and $K\beta''$ lines relative to the $K\beta_{1,3}$ line were extracted. The influence of self-absorption in thick targets was investigated using related x-ray-absorption near-edge-structure spectra that are available in the literature to extract mass absorption coefficients close to the K absorption edge. The correlation of the relative position of the $K\beta_{2,5}$ line with a titanium formal oxidation state in oxide compounds confirmed that the oxidation state of Ti in FeTiO₃ is probably a mixture of Ti III and Ti IV states, which has been recently reported by other authors using different methods. The strengths of the $K\beta_{2,5}$ and $K\beta''$ transition probabilities per titanium-ligand pair were found to decrease exponentially as the average titanium-ligand bond distance increased, which is similar to results obtained for various compounds with vanadium or manganese as the central $3d$ metal atoms.

DOI: [10.1103/PhysRevA.80.042519](https://doi.org/10.1103/PhysRevA.80.042519)

PACS number(s): 33.20.Rm, 36.20.Kd, 78.70.En, 82.80.Ej

I. INTRODUCTION

Numerous studies have been performed to investigate the possibility of using various properties of measured $K\alpha$ and $K\beta$ x-ray bands for chemical speciation. These studies have included the use of the following properties: (i) $K\alpha$ and $K\beta$ x-ray energy shifts [1,2] or $K\beta/K\alpha$ intensity ratios [3–10] as measured with solid-state x-ray detectors, and (ii) energy shifts or intensity ratios of one or more individual $K\alpha$ and $K\beta$ x-ray band components [11–13] as measured with high-energy-resolution crystal spectrometers. It is common for the energies of both the $K\alpha_1$ and $K\alpha_2$ emission lines for transition-metal elements to increase as the oxidation number decreases [14]. Fukushima *et al.* [15] recently analyzed the valence state of Ti in FeTiO₃ with high-resolution x-ray spectroscopy and reported that the energies of both the $K\alpha_1$ and $K\alpha_2$ emission lines increased as the oxidation state of Ti decreased.

It is known that, for the elements in the second and third rows of the periodic table, the intensity distributions of $K\alpha$ x-ray satellites, which arise from the decay of excited states resulting from collisions and containing a single K -shell vacancy and additional L -shell vacancies, are sensitive to the chemical environment of the element [16]. Recently, Watson *et al.* [17] examined the effects of the chemical environment on the intensity distributions and the energies of the $K\alpha$ satellites as well as on the hypersatellite-to-satellite intensity ratios for a number of vanadium oxides.

The chemical bonding of fourth-row transition elements such as Ti involves the $3d$ electrons. This fact has led to extensive investigations of their $K\beta$ x-ray band structures as excited by photons, electrons, and ions in relation to their various chemical compounds. These studies have revealed

significant changes in the relative intensities and positions of the various $K\beta$ x-ray components for different chemical compounds of the same element.

It is also known that the $K\beta_{1,3}$ x-ray emission line of fourth-row transition elements, which arises from the transition of a $3p$ electron to a $1s^{-1}$ core vacancy, is frequently accompanied by a smaller, lower energy satellite $K\beta'$ [18]. This effect was systematically studied by Gamblin and Urch [19] and Peng *et al.* [20] on large sets of transition-metal compounds. Several authors successfully used measurements of the $K\beta'/K\beta_{1,3}$ intensity ratios as sensitive tools for investigating pressure-induced high-spin-to-low-spin transitions in Mn and Fe compounds [21–23]. Another x-ray feature, in addition to $K\beta'$, is observed at energies slightly below the $K\beta_{1,3}$ peak. That is a radiative KMM Auger satellite with a maximum at about 100 eV below the $K\beta_{1,3}$ peak. For Ti metal, Budnar *et al.* [24] reported the yield of the radiative Auger satellite to be about 2.4% relative to the $K\beta_{1,3}$ intensity. Kawai *et al.* [25] investigated the chemical effects on the radiative Auger satellite for a number of Ti compounds. Lépy *et al.* [26] and Campbell *et al.* [27] studied the influence of the radiative Auger satellite and other second-order contributions on the analysis of $K\beta$ and $K\alpha$ x-ray peaks as measured by Si(Li) detectors and other solid-state detectors often used in x-ray spectrometry.

At energies above the $K\beta_{1,3}$ x-ray emission line, several other features are visible by high-energy-resolution crystal spectrometers, including the $K\beta''$, $K\beta_{2,5}$, and $K\beta L^1$ x-ray contributions. There is a common understanding that the $K\beta L^1$ line, which is sometimes referred to as $K\beta'''$ line, can be identified as the $K\beta_{1,3}$ diagram line emitted with one additional L -shell spectator vacancy. Since the energy of $K\beta L^1$ is at the K absorption edge, the influence of its self-absorption is very high. Its intensity is also related to the ratios of the cross section for double (multiple) ionizations, σ_{KL} , to the cross section for single ionization, σ_K . This fur-

*lukam@riteh.hr

TABLE I. A list of measured materials with some basic data used in data analysis. References in the last column were used for average bond lengths.

Sample	Oxidation state	Bond	No. of bonds	Average bond length (nm)	Ref. no.
Ti		Ti—Ti	12	0.2924	[31]
TiO	2	Ti—O	6	0.2089	[31]
Ti ₂ O ₃	3	Ti—O	6	0.2042	[32]
TiO ₂	4	Ti—O	6	0.1959	[33]
MgTiO ₃	4	Ti—O	6	0.1979	[34]
FeTiO ₃	3,4 ^a	Ti—O	6	0.1982	[35]
TiC	4	Ti—C	6	0.2160	[36]
TiN	3	Ti—N	6	0.2120	[37]
TiB ₂		Ti—B	6	0.2350	[38]

^aAccording to Fukushima *et al.* [15] oxidation state of Ti in FeTiO₃ is a mixture of Ti III and Ti IV states.

ther masks possible variations of its intensities due to chemical effects.

The $K\beta_{2,5}$ and $K\beta''$ x-ray lines are good candidates for chemically sensitive x-ray emission spectrometry, since they involve transitions from metal valence orbitals hybridized with the ligand $2s$ and $2p$ states. The peak related to the ligand $2s$ state, $K\beta''$, is sometimes referred to as crossover x-ray emission [12]. $K\beta_{2,5}$ feature includes contributions related to transitions from metal valence orbitals hybridized with the ligand $2p$ states [12]. Bergmann *et al.* [28] measured the high-resolution $K\beta$ x-ray band spectra of a number of Mn compounds, with a focus on the analysis of the $K\beta''$ and $K\beta_{2,5}$ x-ray lines. In the case of Mn oxide compounds, they reported an exponential relationship between the relative intensities of $K\beta''$, which were normalized to the intensity of $K\beta_{1,3}$ and divided by the number of oxygen atoms on the central Mn ion (i.e., number of vanadium-oxygen pairs), as a function of the average manganese-oxygen distance. They concluded that $K\beta''$ and $K\beta_{2,5}$ transitions may be a promising tool for the structural characterization of transition-metal complexes.

Inspired by their work, we decided to investigate the chemical dependence of the relative energies and intensities of the $K\beta$ x-ray band lines for various compounds of other fourth-row transition metals, with a focus on the relative intensities and positions of the $K\beta''$ and $K\beta_{2,5}$ x-ray lines. In our previous study, we investigated the relative energies and intensities of the $K\beta$ band x-ray lines of vanadium compounds [29]. We observed an exponential relationship similar to the one observed by Bergmann *et al.* [28] for the $K\beta''$ x-ray line of Mn oxides, and we also observed similar relationships for $K\beta_{2,5}$ and $K\beta'' + K\beta_{2,5}$ normalized intensities. In the present work, we focused our analysis on titanium compounds with the aim of comparing our observations with those obtained earlier on vanadium compounds. Our future goal is to perform additional measurements on chromium and manganese compounds in order to have a large enough database of measured $K\beta$ x-ray band intensities in which all the measurements were performed under similar experimental conditions and in which all data analysis was performed in a similar way. We intend to use this database to compare

the relative positions and intensities of the $K\beta''$ and $K\beta_{2,5}$ x-ray lines for various transition metals in similar compounds. Similar measurements are scattered in the literature; however, since the reported values were obtained using different methods of data analysis or using different excitation conditions, it is difficult to use them for comparison. This may be of importance, because it was observed as early as the 1970s that the $K\beta/K\alpha$ intensity ratios depend on the mode of excitations [30]. Our analysis is concentrated on x-ray excitation by charged particles [particle-induced x-ray emission (PIXE)].

II. EXPERIMENTAL METHODS AND DATA ANALYSIS

A. Experimental methods

The measurements of the $K\beta$ band x-ray spectra were performed at the Laboratory for Ion Beam Interactions of the Rudjer Bošković Institute, Zagreb. Most of the experimental details were the same as those described in [29]. All the targets were bombarded with 2 MeV protons provided by a 1 MV Tandetron electrostatic accelerator. The targets consisted of a thick foil of metallic titanium and thick, compressed pellets made up of the materials listed in Table I. Table I also presents some basic data used in the data analysis. The pellets were compressed from high-purity powders obtained from Aldrich Chemical Co., Inc., Milwaukee, WI.

The incident-proton beam and x-ray emission angle were set both to an angle of 45° with respect to the target surface. A flat LiF(110) crystal was used as a wavelength dispersive element, and a position-sensitive proportional counter (PSPC) was used as a detector. The total distance between the target and the detector was 60 cm. The given geometry of the detector system provided 4.4 eV/mm spatial energy distribution along the position-sensitive axis of the detector at the position of the Ti $K\beta_{1,3}$ x-ray line. The resolution of the detector system was limited by the effective x-ray source size as seen by the detector. The effective x-ray source size is defined by the proton beam collimation system and the beam-target-detector angles. In our measurements, the effective x-ray source size was 0.8 mm, which corresponds to 3.5

eV in energy units. The detected spectral lines had natural Lorentzian profiles convoluted with the spatial proton beam intensity profile. The full width at half maximum (FWHM) of the profile was equal to 3.5 eV in energy units. Line broadening due to the detector was also present but is less important. However, the Ti $K\beta_{1,3}$ line was measured with a FWHM equal to 5.4 eV, which was enough for the $K\beta_{2,5}$ and $K\beta''$ lines to be clearly resolved with some exceptions for Ti_2O_3 and TiO. The spectra were collected using our in-house developed data acquisition and analysis system, SPECTOR [39,40].

B. Data analysis

We first used a similar approach to the data analysis performed in our previous work on vanadium and its compounds [29]. All the measured spectra were fitted using the wxEWA (V0.29a-Alpha8) least-squares fitting program [41]. The $K\beta'$, $K\beta_{1,3}$, $K\beta''$, and $K\beta_{2,5}$ x-ray lines were described as pseudo-Voigt functions, and the radiative Auger and $K\beta L^1$ contributions were represented by Gaussian functions. We introduced another residual pseudo-Voigt peak $K\beta_{res}$ between the $K\beta'$ and $K\beta_{1,3}$ peaks, following the approach used by Gamblin and Urch [19]. The background was represented by a linear function with a negative slope. Energy calibration was performed from spectra related to measured titanium metal samples and was based on energies for the $K\beta_{1,3}$ and $K\beta_{2,5}$ x-ray lines that were reported by Bearden [42]. Figure 1 shows all the measured and fitted spectra, which are aligned relative to the position of the $K\beta_{1,3}$ peak centroid.

Afterward, line intensities were corrected for self-absorption in a thick target. In Fazinić *et al.* [29], we made this correction using the TTPIXAN code [43] to calculate theoretical thick target PIXE yields for selected x-ray energies. For that purpose we have upgraded the TTPIXAN database with estimated mass absorption coefficients close to the K absorption edge, which were extracted from reported, experimental x-ray-absorption-near-edge spectra (XANES). In the present work, we have developed our own code and used it to calculate a theoretical thick-to-thin target relative yield function, Y_r , for the range of energies covered by our spectra. In these calculations, we used proton stopping-power data from SRIM code [44], K -shell ionization cross sections from Chen and Crasemann [45], and mass absorption coefficients that were extracted from XANES spectra [46–57] and were normalized to the database of Hubbell and Seltzer [58]. Figure 2 shows the mass attenuation coefficients for all the sample materials used in this work.

Figure 3 shows the calculated, normalized thick-to-thin target relative yield function, $Y_r(E)$, for the following conditions: a Ti metal sample, 2 MeV protons, our measurement geometry, and an x-ray energy range close to the K absorption edge. In order to make Y_r applicable to our spectrum fits, we have convoluted Y_r with the spectral response function of our detector system, which, according to our experimental setup, is approximated as a Gaussian function with a FWHM of 4.0 eV. The fine structure of this absorption edge, which has a pre-edge peak at about 4965.5 eV [49] (see Fig. 2) is reflected in this function as a reverse peak. It is partly

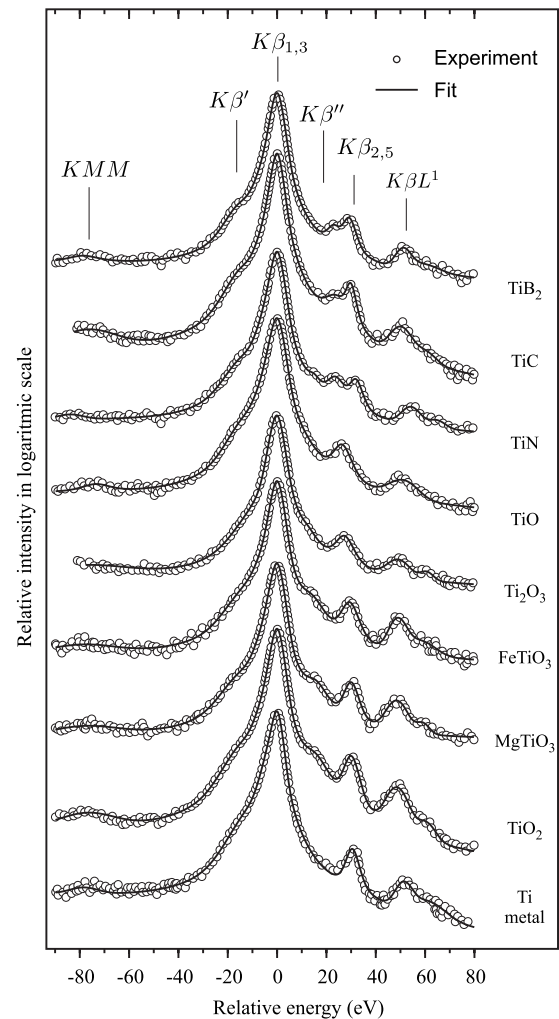


FIG. 1. The measured and fitted spectra of all the samples. The spectra are aligned relative to the position of the $K\beta_{1,3}$ peak centroid.

smear out in our measurements due to the low spectral resolution of our measurement system. The reciprocal function, $1/Y_r$, represents thick-to-thin target corrections, which we used to report our final results for relative peak intensities. As an example, we can conclude from Fig. 3 that, for the metallic Ti target ($K\beta_{1,3}$ located at about 4932 eV and $K\beta L^1$ at about 4980 eV), the thick-target $K\beta L^1/K\beta_{1,3}$ intensity ratio will be at 24% of the level of the thin target $K\beta L^1/K\beta_{1,3}$ intensity ratio. Thus, our experimentally measured $K\beta L^1/K\beta_{1,3}$ yield ratio should be multiplied by the reciprocal value (i.e., a correction factor of 4.2) to obtain the $K\beta L^1/K\beta_{1,3}$ intensity ratio that corresponds to a thin target. Figure 3 also shows that the correction factors for the $K\beta'/K\beta_{1,3}$ intensity ratios ($K\beta'$ is located at about 10 eV lower than $K\beta_{1,3}$) and the $K\beta''/K\beta_{1,3}$ intensity ratios ($K\beta''$ is located well below 4960 eV) are negligible. For the $K\beta_{2,5}/K\beta_{1,3}$ intensity ratios, the value of the correction factor critically depends on the position of the pre-edge peak in the XANES spectrum and on the profile of the mass attenuation coefficients. The comparison of a few XANES data sources [48–57] has shown calibration shifts up to 3 eV for metallic titanium and even 8 eV for TiO_2 (rutile), which are

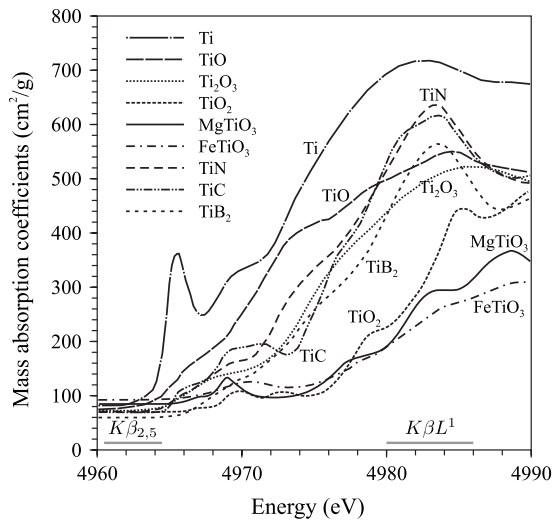


FIG. 2. The mass absorption coefficients for measured materials that were estimated from the corresponding XANES spectra [46–57] and tabulated data [58] before and after the absorption edge. At the bottom, the typical ranges of affected emission lines are indicated by horizontal bars.

the two most common measured absorbers. Being unsure about which source to trust, we have calculated the average position of characteristic peaks and have found that the values of Tsutsumi *et al.* [49] are very close to these average values. Tsutsumi *et al.* have also reported combined emission and absorption spectra in the $K\beta_{2,5}$ region where high caution in calibration is expected, and we have adopted their calibration as the most reliable.

Figure 4(a) shows the normalized thick-to-thin target relative yield function, Y_r , for a Ti metal sample with measurements at five different proton energies between 1 and 3 MeV. The thick-to-thin target yield for the $K\beta L^1/K\beta_{1,3}$ intensity ratios decreases considerably with increasing energy. Figure 4(b) shows Y_r functions for Ti metal, TiO_2 , and $FeTiO_3$ that were calculated for incoming 2 MeV protons. This figure illustrates that the correction factors, $1/Y_r$, are generally

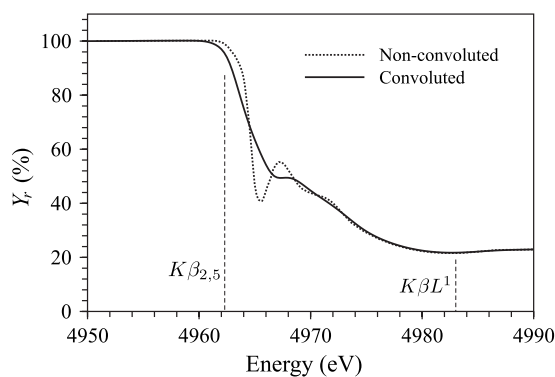


FIG. 3. The normalized thick-to-thin target relative yield function in the K -edge region for a thick Ti foil target bombarded with 2 MeV protons in our measurement geometry (dotted line) and associated convolution obtained using the spectral response function of our spectrometer (full line). The positions of the $K\beta_{2,5}$ and $K\beta L^1$ emission lines are emphasized.

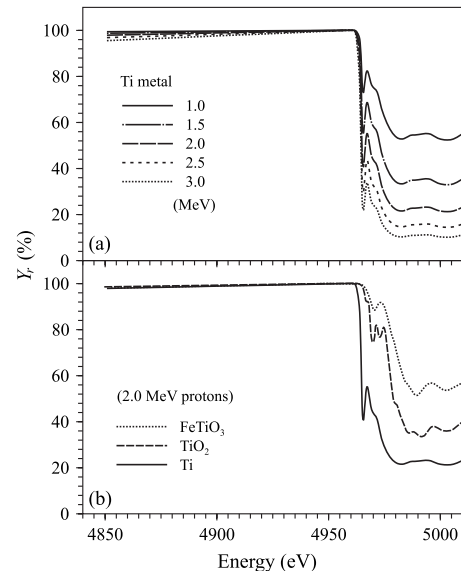


FIG. 4. The normalized thick-to-thin relative yield function for a) a thick Ti foil target bombarded with 1, 1.5, 2, 2.5, and 3 MeV protons and for b) thick Ti metal, TiO_2 (rutile), and $FeTiO_3$ targets bombarded with 2 MeV protons.

smaller for the measured titanium compounds compared to titanium metal. There are two reasons for such behavior: the stopping power for protons is larger in oxides due to an increased concentration of weakly bound electrons, which reduces the proton range, and the mass absorption coefficients are smaller due to a decreased concentration of Ti atoms. Figure 4(b) also shows that the correction factors, $1/Y_r$, will still be relatively high for the $K\beta L^1/K\beta_{1,3}$ intensity ratios, whereas the correction factors related to the $K\beta_{2,5}/K\beta_{1,3}$ intensity ratios are much smaller for measured compounds and are at the level of 1.01–1.02. This is mostly affected by different energy profiles of the mass attenuation coefficients in the vicinity of the $K\beta_{2,5}$ peaks in the measured compounds. The pre-edge peak, which is strong in the case of metallic titanium, is weak or missing for all the measured compounds. Our measurements and those of others showed that $K\beta_{2,5}$ peaks are positioned at lower energies than those of metallic titanium, and the rise in mass attenuation coefficients starts at the higher energies. The consequence of this is relatively large $K\beta_{2,5}/K\beta_{1,3}$ intensity ratio correction factor of 1.31 for the Ti metal and almost negligible correction factor for the measured compounds.

The thick-to-thin target relative yield function, Y_r , is useful for graphical presentations because it approximates the shape of the thick-target PIXE background in our experimental conditions. When the measured background of the $K\beta$ x-ray spectra at about 150 eV, in the vicinity of K edge, is fitted with a sloped line, it overestimates the real background at the energies above the K edge, and it underestimates the real background at the energies below the K edge (see Fig. 5). Since both the $K\beta_{2,5}$ and $K\beta L^1$ x-ray lines are located within this critical energy region, inappropriate treatment of the background may affect the reported, fitted intensities.

In order to clarify this issue, we have developed an alternative model of spectral and data analysis, which is partly

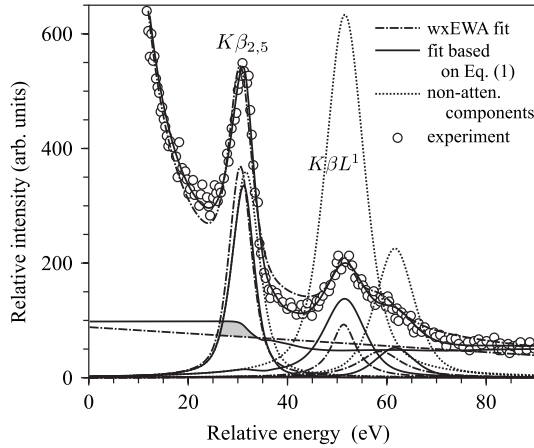


FIG. 5. The fit of the K -edge region of the measured $K\beta$ spectrum for a metallic titanium sample. The zero value of the relative energy corresponds to the $K\beta_{1,3}$ centroid (4931.8 eV).

based on the approach described by Kavčič *et al.* [13] and Uršič *et al.* [59]. In their data analysis, they first corrected the spectra that were obtained from thick targets by calculating thick-to-thin target x-ray yield correction factors channel by channel. In their work, they used mass attenuation coefficients in the form of a step convoluted with their spectrometer response function. Then, the corrected spectra were fitted using a standard least-squares fitting program.

In our alternative approach, the originally measured spectra were fitted to the following model function:

$$s(E) = \left[a + \sum_{i=1}^n P_i(A_i, E_i, w_i, m_i, E) \right] Y_r(E) + b, \quad (1)$$

where P_i stands for the measured x-ray peaks, A_i is the amplitude, E_i is the centroid energy, w_i is the FWHM, and m_i is the Lorentzian-Gaussian mixing parameter. In this model function, the measured x-ray peaks are represented, as in our first approach, by pseudo-Voigt and Gaussian functions ($m_i = 0$). The background is described as a horizontal line divided into two parts, of which the first one (designated as a) is associated with PIXE bremsstrahlung attenuated in the sample and the second one (designated as b) is associated with the electronic noise and has no origin in the sample itself. The first part of the background and x-ray peaks are multiplied with the theoretically calculated normalized thick-to-thin target relative yield function, $Y_r(E)$, as already described.

Compared to the first simpler model, this model achieves much better agreement between the measured data and the fit in the energy regions below and above the $K\beta_{2,5}$ x-ray peak for the thick Ti metallic target spectra. As we already observed in [29], we could not properly fit the spectra measured from the thick vanadium metal foil using a simple model without having to introduce a peak at a position slightly below the $K\beta_{2,5}$ peak. We encountered the same problem when fitting the spectra measured from the thick titanium metal foil; however, fitting the spectra with the model given in Eq. (1) considerably improved the quality of fit in this region without the introduction of a peak at the position slightly

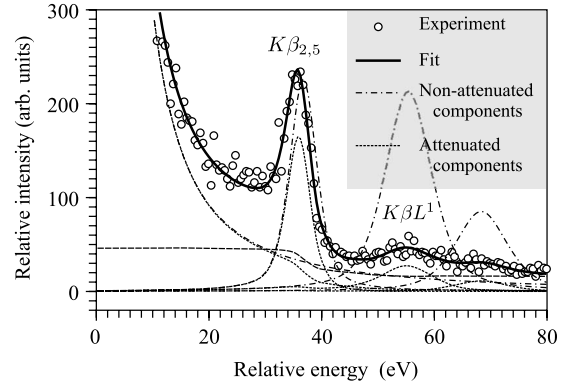


FIG. 6. The fit of the K -edge region of the measured $K\beta$ spectrum for a metallic vanadium sample. The zero value of the relative energy corresponds to the $K\beta_{1,3}$ centroid (5427.3 eV).

below the $K\beta_{2,5}$ peak. Figures 5 and 6 show higher energy portions of titanium and vanadium metal spectra, respectively, and they show experimental data, individual fitted lines ($K\beta_{2,5}$ and $K\beta L^1$), and the fitted results obtained by both models. The problem is not as apparent when fitting spectra for Ti compounds with the simple approach (fitting raw spectra and then correcting resulting peak areas with correction factors obtained as $1/Y_r$) because, as Fig. 4(b) shows, the influence of the K edge on Y_r close to the position of the $K\beta_{2,5}$ x-ray peak is not as high for Ti compounds as for Ti metal.

Both models resulted in similar relative peak areas, which are statistically the same when estimated overall uncertainties are taken into account. Thus, since we intend to make further measurements of chromium and manganese compounds and since we have already made measurements on vanadium compounds and analyzed them using the first model (wxEWA+ $1/Y_r$ correction factors), all of the results on the relative $K\beta''$ and $K\beta_{2,5}$ intensities from the titanium compounds that are reported in this study were obtained using the first model. However, the results for the Ti metal were obtained by the method based on Eq. (1).

III. RESULTS AND DISCUSSION

The results obtained from the analysis of the measured spectra are summarized in Table II. This table shows the measured positions of the $K\beta''$ and $K\beta_{2,5}$ x-ray lines relative to the fitted position of the $K\beta_{1,3}$ peak centroid and the energy difference between the $K\beta''$ and $K\beta_{2,5}$ x-ray lines. The table also shows the relative intensities of these two lines with respect to the low-energy region of the $K\beta$ x-ray band, i.e., to the sum of the $K\beta'$, $K\beta_{re}$, and $K\beta_{1,3}$ x-ray intensities. The table also shows experimental data from the available literature. We are not reporting the positions and intensities of the $K\beta'$ line relative to the $K\beta_{1,3}$. Based on extensive measurements of a number of compounds with $3d$ elements, Gamblin and Urch [19] recently concluded that the relative positions and intensities of the $K\beta'$ line could be good measure for chemical effects for Cr and Mn compounds, whereas this is not the case for low- Z elements mainly due to experimental limitations. In the case of Ti compounds, the $K\beta'$ line

TABLE II. The energy differences and intensities relative to the sum $K\beta_{1,3}+K\beta_{res}+K\beta'$. Other experimental results from the literature are also presented.

Sample	ΔE (eV)			I_{rel} (%)		
	$(K\beta''-K\beta_{1,3})$	$(K\beta_{2,5}-K\beta_{1,3})$	$(K\beta_{2,5}-K\beta'')$	$K\beta''$	$K\beta_{2,5}$	$K\beta''+K\beta_{2,5}$
Ti	-	30.5 [42]	-	-	1.98 ± 0.63 1.86 ± 0.71 [59] 2.02 [61] 2.53 ± 0.40 [62]	1.98 ± 0.63
TiO	^a	26.3 ± 0.5 25.9 ^b [49]	^a 15.7 [63] 15.5 ^b [64] 15 ^b [65]	0.74 ± 0.08	3.11 ± 0.28	3.85 ± 0.29
Ti ₂ O ₃	^a	27.8 ± 0.5	^a	1.50 ± 0.15	3.75 ± 0.35	5.25 ± 0.38
FeTiO ₃	13.9 ± 0.2	28.9 ± 0.5	15.0 ± 0.5	3.91 ± 0.39	3.80 ± 0.38	7.71 ± 0.54
TiO ₂	15.1 ± 0.2	29.8 ± 0.5 30 ^b [49] 30.4 [67] 29.7 ^b [69]	14.7 ± 0.5 15.6 [66] 15.4 ^b [68] 15.2 [67]	3.86 ± 0.38	3.52 ± 0.35	7.38 ± 0.52
MgTiO ₃	15.5 ± 0.2	29.9 ± 0.5	14.4 ± 0.5	3.16 ± 0.32	3.27 ± 0.33	6.43 ± 0.46
TiB ₂	22.3 ± 0.2	29.2 ± 0.5	6.9 ± 0.5	1.26 ± 0.13	2.61 ± 0.26	3.87 ± 0.29
TiC	22.1 ± 0.2	29.3 ± 0.5	7.2 ± 0.5 7.2 [64] 8.2 [70] 7 [71,72]	1.44 ± 0.15	2.86 ± 0.29	4.30 ± 0.33
TiN	23.3 ± 0.2	31.6 ± 0.5	8.3 ± 0.5 10 [71] 11.3 [72,70]	2.19 ± 0.30	2.22 ± 0.30	4.41 ± 0.42

^a $K\beta''$ not resolved (position parameter linked to $K\beta_{2,5}$).

^bPosition of $K\beta_5^I$ taken to represent $K\beta_{2,5}$.

is seen only as a low-energy shoulder (see Fig. 1) which we described with one pseudo-Voigt function. In reality, the $K\beta'$ line is a complex sum of multiplet lines and an analysis of its structure would require complex theoretical calculations with multiplet terms [20,60]. To a certain extent, the $K\beta''$ and $K\beta_{2,5}$ x-rays are also unresolved multiplets, but they have much better defined forms with clearly seen centroid positions and shapes which we approximated with one pseudo-Voigt profile, having in mind the strategy to analyze the spectra with minimal number of model peaks needed to obtain good fits (following the procedure explained in the previous chapter). This is the best compromise that we could do to obtain as reliable data as possible for the given purpose.

A. Relative positions of the $K\beta''$ and $K\beta_{2,5}$ x-ray lines

The first columns of Table II show the following measured energy differences: $\Delta E(K\beta''-K\beta_{1,3})$, $\Delta E(K\beta_{2,5}-K\beta_{1,3})$, and $\Delta E(K\beta_{2,5}-K\beta'')$. As the positions of related lines in measured spectra are well defined, statistical uncertainties of varied centroid parameters calculated by the spectral analysis fit code are small (0.1–0.2 eV). However, we reported errors of 0.5 eV in the case of compounds due to investigated influence of self-absorption and possible errors

related to XANES spectra calibration uncertainties. In the case of pure metal, distortion of $K\beta_{2,5}$ peak profile at its high-energy side is even stronger because of the closely positioned sharp pre-edge peak in XANES spectrum, leading to the estimated error up to 1 eV for the position of the $K\beta_{2,5}$ centroid. Most of the experimental data in the available literature relate to the relative energy difference of the $K\beta_{2,5}$ and $K\beta''$ lines; however, almost all of the data are presented as spectra in a graphical form, and the values given in Table II have been extracted from such published spectra if the related energy scale was given. Bergmann *et al.* [28] showed that, for manganese oxide compounds, the $K\beta_{2,5}$ main peak energies increase linearly with the formal oxidation state of manganese. Fazinić *et al.* [29] showed that the energy difference between the $K\beta_{2,5}$ and $K\beta_{1,3}$ lines increase with the formal oxidation state of vanadium for a number of vanadium compounds. In their recent work, Fukushima *et al.* [15] performed the valence state analysis of Ti in FeTiO₃ (ilmenite) by measuring high-resolution x-ray spectra (e.g., Ti $K\alpha_{1,2}$, Ti $L\alpha_{1,2}$, and O $K\alpha$) in several Ti compounds with known Ti valence states and by comparing the corresponding spectra with those for FeTiO₃. The Ti compounds that they used have known valence states such as Ti₂O₃ (Ti III), TiO₂ (Ti IV), and MgTiO₃ (Ti IV). The measurements were carried

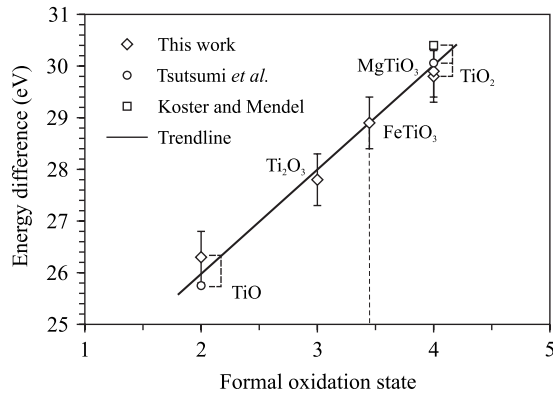


FIG. 7. The dependence of the measured energy difference between $K\beta_{2,5}$ and $K\beta_{1,3}$ on the formal oxidation state of measured oxides. The results are supported by data found in the literature [49,67].

out using a high-resolution wavelength x-ray fluorescence spectrometer with an electron probe microanalyzer. Earlier measurements of FeTiO_3 (ilmenite) based on Mössbauer spectroscopy suggested that the oxidation state of Fe is Fe II. These measurements lead to the conclusion that the oxidation state of Ti should be Ti IV, which is the same for TiO_2 . As a result of their analysis, Fukushima *et al.* concluded that the valence state of Ti in FeTiO_3 (ilmenite) was at least partially Ti III and might be the mixed state of Ti IV and Ti III. They supported this conclusion with a high-energy excitation XPS experiment. They also confirmed that Ti in MgTiO_3 (ilmenite system) is Ti IV. In this work, we measured the $K\beta$ x-rays for the same Ti compounds with known formal oxidation states that Fukushima *et al.* used: Ti_2O_3 (Ti III), TiO_2 (Ti IV), and MgTiO_3 (Ti IV). We also measured $K\beta$ x-rays for TiO (Ti II). Figure 7 shows that the measured $K\beta_{2,5}-K\beta_{1,3}$ energy difference is linearly proportional to the formal oxidation state of these Ti oxides. The figure shows our measured results and those found in the available literature for TiO and TiO_2 . The figure also shows our results for the $K\beta_{2,5}-K\beta_{1,3}$ energy difference of FeTiO_3 . Our results suggest that the formal oxidation state of Ti in FeTiO_3 falls around 3.4–3.5, which is in line with the conclusion of Fukushima *et al.*

The analysis of titanium metal spectra with the model based on Eq. (1) showed that there is no need to introduce a peak between the $K\beta_{1,3}$ and $K\beta_{2,5}$ x-rays (i.e., $K\beta''$). Therefore Table II does not report any data on the $K\beta''$ x-ray line for titanium metal. Our measured TiO and Ti_2O_3 spectra show that the $K\beta''$ components are not visible; however, there are several reports in the available literature about the existence of the $K\beta''$ line in TiO. Ern and Switendick [63] and Fischer [64] showed clearly resolved $K\beta''$ and $K\beta_{2,5}$ peaks for TiO, from which the relative energy differences were extracted and found to be 15.7 and 15.5 eV, respectively. The compilation done by Fazinić *et al.* [29] shows that the measured energy difference between the $K\beta_{2,5}$ and $K\beta''$ lines varies between 13.6 and 16.5 eV for a range of 3d metal oxides (Ti, V, Cr, Mn, and Fe). Since $\Delta E(K\beta_{2,5}-K\beta_{1,3})$ increases with the formal oxidation state (see Fig. 7) and since its value is 26.3 eV for TiO (see Table II), the

position of the $K\beta''$ x-ray line would be only 10.7 eV from the $K\beta_{1,3}$ peak centroid. The low intensity of this peak compared to the intensity of the $K\beta_{1,3}$ peak could be the main reason why the $K\beta''$ line is not visible for TiO and Ti_2O_3 . Therefore, in fitting the TiO and Ti_2O_3 spectra, we introduced a $K\beta''$ peak at a position that is 15.6 eV below the $K\beta_{2,5}$ peak. We linked the width of this peak to the width of the $K\beta_{2,5}$ peak, using the spectra published by Ern and Switendick [63] and Fischer [64]. The relative intensities of the $K\beta''$ peak obtained in such a way for TiO and Ti_2O_3 are reported in Table II.

B. Relative intensities of the $K\beta''$, $K\beta_{2,5}$, and $K\beta L^1$ x-ray lines

Table II shows our experimental results for the relative positions and intensities of the $K\beta''$ and $K\beta_{2,5}$ lines and all the data found in the available literature. Unlike for the other 3d metal compounds, there are not many reports providing numerical data about the relative intensities and energies of these x-ray lines for titanium compounds. We could not find any reported experimental data related to the relative intensities of the $K\beta''$ and $K\beta_{2,5}$ lines for the titanium compounds that are analyzed in this work. The situation is slightly better for titanium metal. The results for the relative intensities of the $K\beta''$ and $K\beta_{2,5}$ lines, which are reported in Table II, were obtained using the simple approach of fitting the raw spectra with wxEWA and then correcting for thick-target self-absorption with the help of the $1/Y_r$ correction factors. The one exception is titanium metal, for which the results for the relative intensities of the $K\beta_{2,5}$ line, which are reported in Table II, were obtained using the model based on the Eq. (1). Our result of 1.98% is in very good agreement with the values reported by Uršič *et al.* [59] (1.86%) and Török *et al.* [61] (2.02%). The result reported by Kavčič *et al.* [62] (2.53%) is slightly larger than ours, but they report the intensities of the $K\beta_{2,5}$ line relative to the $K\beta_{1,3}$ line and fitted the spectra as only one line. All of the authors analyzed their spectra using an approach similar to our model based on Eq. (1). We also reanalyzed vanadium metal spectra described in [29] in a similar way. In [29], we analyzed the vanadium metal spectrum with the assumption that there is a $K\beta''$ peak on the low-energy side of the $K\beta_{2,5}$, and we reported the relative intensities of both of these peaks. Here, we are reporting the re-evaluated relative intensity of the $K\beta_{2,5}$ line for metallic vanadium as $(2.4 \pm 0.3)\%$, which was obtained using the model based on Eq. (1) and without using the $K\beta''$ peak. This value is significantly different than the value published in [29], but it is similar to the reported sum of the $K\beta_{2,5}$ and $K\beta''$ intensities (2.27%).

Bergmann *et al.* [28] found that, for oxygen-ligated Mn compounds, the measured strength of the $K\beta''$ transition (presented with its intensity normalized to the intensity of $K\beta_{1,3}+K\beta''$ and divided by the number of Mn-O bonds per the central Mn atom) decreases exponentially with increasing average Mn-O bond distance. They explained that this behavior is a consequence of the $K\beta''$ transition originating in the mixed state of the metal p and oxygen $2s$ atomic orbitals, in which the amount of mixing will depend, according to perturbation theory, on the overlap of the corresponding

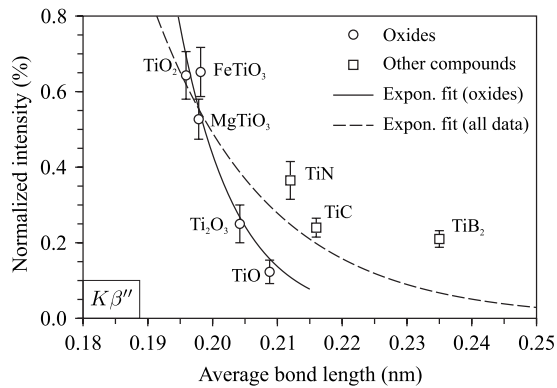


FIG. 8. The relative intensities of the $K\beta''$ x-ray line normalized to the intensity of $K\beta_{1,3}+K\beta_{res}+K\beta'$ and divided by the number of ligands per the central titanium ion (i.e., the number of titanium-ligand pairs) as a function of the average titanium-ligand distance.

wave functions. Since these wave functions have exponentially decreasing tails, it is expected that the amount by which they overlap will also decrease as the interatomic distance increases. In our analysis of the relative intensities of the $K\beta''$ and $K\beta_{2,5}$ lines for vanadium compounds [29], it was shown that normalized intensities of the $K\beta_{2,5}$ x-ray line and the sum of their normalized intensities, $K\beta''+K\beta_{2,5}$, also have similar a dependence on the average metal-ligand bond distance.

Figures 8–10 show the dependence of the $K\beta''$, $K\beta_{2,5}$, and $K\beta''+K\beta_{2,5}$ intensities, which were normalized to the intensity of the $K\beta_{1,3}+K\beta_{res}+K\beta'$ x-ray lines and were divided by the number of Ti-ligand bonds per the central Ti atom, versus the average bond length between the central Ti atom and the ligand atoms. The normalized intensities in all three graphs generally decrease as the average bond length increases. Two exponential trend lines for the $K\beta''$ normalized intensities are also presented. One of the trend lines approximates the data belonging to oxides, and the other approximates the whole set of data. The results suggest that the decrease of normalized intensities with the increase of the average bond length is more rapid in oxides. Figure 9 shows

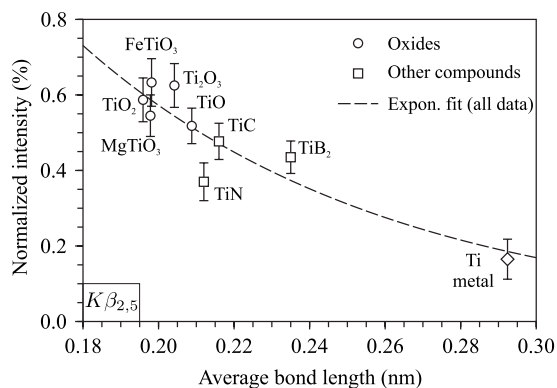


FIG. 9. The relative intensities of the $K\beta_{2,5}$ x-ray line normalized to the intensity of $K\beta_{1,3}+K\beta_{res}+K\beta'$ and divided by the number of ligands per the central titanium ion (i.e., the number of titanium-ligand pairs) as a function of the average titanium-ligand distance.

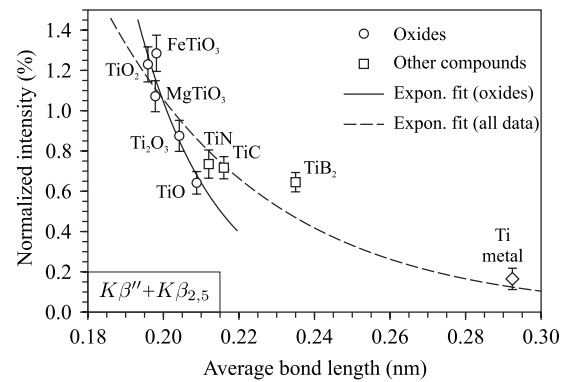


FIG. 10. The relative intensities of $K\beta''+K\beta_{2,5}$ x-ray lines normalized to the intensity of $K\beta_{1,3}+K\beta_{res}+K\beta'$ and divided by the number of ligands per the central titanium ion (i.e., the number of titanium-ligand pairs) as a function of the average titanium-ligand distance.

a grouping of data for the normalized intensities of the $K\beta_{2,5}$ line around the exponential trend line for all the measured samples, including the Ti metal. This trend for the normalized intensities of the $K\beta_{2,5}$ line is weaker than the one for the $K\beta''$ line because of the double character of this line; i.e., it is a mixture of a quadrupole x-ray emission from the metal 3d states and a dipole transition from molecular orbitals with metal 4p and oxygen 2p contributions [12].

The $K\beta L^1$ x-ray lines are located at about 50 eV above the $K\beta_{1,3}$ peak, which is at about 4980 eV. Figure 2 shows that there is a large difference in mass absorption coefficients between different samples for x-ray energies of about 4980 eV. The highest mass absorption coefficient of about $700 \text{ cm}^2/\text{g}$ is for Ti metal, and the lowest value of about $200 \text{ cm}^2/\text{g}$ is for MgTiO_3 and FeTiO_3 . This fact has a strong influence on the recorded intensities of the $K\beta L^1$ x-rays from our thick targets. Since thick-to-thin target correction factors depend on mass absorption coefficients, stopping powers of protons in related materials, and ionization cross sections, our analysis is strongly influenced by the large uncertainties in both the mass absorption coefficients for the energies in question and the ratios of cross sections for double ionization, σ_{KL} , to single ionization, σ_K . Figures 3 and 4 show normalized thick-to-thin target relative yield functions based on single-ionization cross sections, σ_K . If we neglect ratios of cross sections for double ionization, σ_{KL} , to single ionization, σ_K , these figures show that, for 2 MeV protons, the thick-target yield of the $K\beta L^1$ x-rays (relative to the $K\beta_{1,3}$ yield) would be about 22% of the thin target yield for Ti metal, 48% for rutile, and 72% for FeTiO_3 . In other words, the thick-target yield ratio, $K\beta L^1/K\beta_{1,3}$ for FeTiO_3 would be for a factor of about 3.3 higher than the respective ratio for Ti metal. A similar result is also expected for MgTiO_3 . Our experimental results for the thick-target yield ratio, $K\beta L^1/K\beta_{1,3}$ for FeTiO_3 is higher than the ratio for Ti metal by a factor of 2.9, and this factor is 3.4 for MgTiO_3 . Taking into account that our results for the intensities of the $K\beta L^1$ line have estimated errors of more than 30%, these measured ratios are in good agreement with the values expected from thick targets. Therefore, any possible variations in $K\beta L^1/K\beta_{1,3}$ intensity ratios due to possible chemical effects

is probably hidden by the effects related to the differences in $K\beta L^1$ self-attenuation of x-rays in different samples, which is due to the large variations of the mass absorption coefficients and the different stopping powers of ions in different materials.

IV. CONCLUSION

High-resolution x-ray spectrometry in combination with PIXE is sensitive enough to determine the oxidation states of titanium in various titanium oxides using the energy difference between the $K\beta_{1,3}$ and $K\beta_{2,5}$ spectral lines. In the non-trivial case of determining the oxidation state of titanium in FeTiO_3 , the presented method indicates that the formal oxidation state is 3.45 ± 0.30 .

The sum of the relative intensities of the $K\beta_{2,5}$ and $K\beta''$ lines, which is normalized per metal-ligand pair, exponentially decreases as the average metal-ligand bond length increases. Until now, investigations have shown that this property is common for measured titanium, vanadium, and manganese compounds. This property can be used for the structural characterization of transition-metal complexes in high-resolution PIXE experiments.

The influence of thick-target self-absorption has been analyzed using XANES spectra from the literature to estimate the mass absorption coefficients close to the K absorption edge. The calculated thick-to-thin target yield function is introduced to upgrade the fit procedure. The spectrum fit results obtained with the upgraded model are better than the results obtained with the method based on the wxEWA software. The main disadvantage of the upgraded approach arose from XANES calibrations that were found to be inconsistent between different sources. The $K\beta L^1$ region in particular cannot be analyzed with high reliability. In titanium compounds, the $K\beta_{2,5}$ line remains basically unaffected by this feature, whereas, for pure titanium, the correction factor for self-absorption depends strongly on the XANES calibration and some reasonable selection from many sources was done to obtain our final results.

The results obtained so far on vanadium and titanium compounds encourage the continuation of similar investigations on other $3d$ metal compounds.

ACKNOWLEDGMENTS

This work was supported by the Croatian Ministry of Science, Education and Sports through Research Projects No. 098-1191005-2876 and No. 069-0691668-3007.

-
- [1] N. Kallithrakas-Kontos and R. Moshohoritou, *X-Ray Spectrom.* **27**, 173 (1998).
- [2] T. Papp, J. L. Campbell, and E. Papp-Szabó, *Nucl. Instrum. Methods Phys. Res. B* **189**, 33 (2002).
- [3] E. Arndt, G. Brunner, and E. Hartmann, *J. Phys. B: At., Mol. Opt. Phys.* **15**, L887 (1982).
- [4] G. Brunner, M. Nagel, E. Hartmann, and E. Arndt, *J. Phys. B: At., Mol. Opt. Phys.* **15**, 4517 (1982).
- [5] T. Mukoyama, K. Taniguchi, and H. Adachi, *Phys. Rev. B* **34**, 3710 (1986).
- [6] C.-N. Chang, C.-T. Chen, C.-C. Yen, and Y.-H. Wu, C.-W. Su, and S.-K. Chiou, *J. Phys. B: At., Mol. Opt. Phys.* **27**, 5251 (1994).
- [7] L. Rebohle, U. Lehnert, and G. Zschornack, *X-Ray Spectrom.* **25**, 295 (1996).
- [8] M. Polasik, *Phys. Rev. A* **58**, 1840 (1998).
- [9] S. Raj, H. C. Padhi, M. Polasik, and D. K. Basa, *Solid State Commun.* **110**, 275 (1999).
- [10] T. Mukoyama, K. Taniguchi, and H. Adachi, *X-Ray Spectrom.* **29**, 426 (2000).
- [11] A. Meisel, G. Leonhards, and R. Szargan, *X-Ray Spectra and Chemical Binding* (Springer-Verlag, Berlin, Heidelberg, New York, 1989).
- [12] F. deGroot, *Chem. Rev. (Washington, D.C.)* **101**, 1779 (2001).
- [13] M. Kavčič, A. G. Karydas, and C. Zarkadas, *X-Ray Spectrom.* **34**, 310 (2005).
- [14] Y. Gohshi, *X-Ray Spectrom.* **4**, 117 (1975).
- [15] S. Fukushima, T. Kimura, K. Nishida, V. A. Mihai, H. Yoshikawa, M. Kimura, T. Fujii, H. Oohashi, Y. Ito, and M. Yamashita, *Mikrochim. Acta* **155**, 141 (2006).
- [16] R. L. Watson, T. Chiao, and F. E. Jenson, *Phys. Rev. Lett.* **35**, 254 (1975).
- [17] R. L. Watson, V. Horvat, and Y. Peng, *Phys. Rev. A* **78**, 062702 (2008).
- [18] L. G. Parratt, *Rev. Mod. Phys.* **31**, 616 (1959).
- [19] S. D. Gamblin and D. S. Urch, *J. Electron Spectrosc. Relat. Phenom.* **113**, 179 (2001).
- [20] G. Peng *et al.*, *J. Am. Chem. Soc.* **116**, 2914 (1994).
- [21] J. Badro, J. P. Rueff, G. Vankó, G. Monaco, G. Fiquet, and F. Guyot, *Science* **305**, 383 (2004).
- [22] C. S. Yoo *et al.*, *Phys. Rev. Lett.* **94**, 115502 (2005).
- [23] J.-F. Lin, V. V. Struzhkin, S. D. Jacobsen, M. Y. Hu, P. Chow, J. Kung, H. Liu, H.-K. Mao, and R. J. Hemley, *Nature (London)* **436**, 377 (2005).
- [24] M. Budnar, A. Mühleisen, M. Hribar, H. Janžekovič, M. Ravnikar, Ž. Šmit, and M. Žitnik, *Nucl. Instrum. Methods Phys. Res. B* **63**, 377 (1992).
- [25] J. Kawai, T. Nakajima, T. Inoue, H. Adachi, M. Yamaguchi, K. Maeda, and S. Yabuki, *Analyst (Cambridge, U.K.)* **119**, 601 (1994).
- [26] M. C. Lépy, J. Plagnard, and J. Morel, *Nucl. Instrum. Methods Phys. Res. A* **339**, 241 (1994).
- [27] J. L. Campbell, J. A. Maxwell, T. Papp, and G. White, *X-Ray Spectrom.* **26**, 223 (1997).
- [28] U. Bergmann, C. R. Horne, T. J. Collins, J. M. Workman, and S. P. Cramer, *Chem. Phys. Lett.* **302**, 119 (1999).
- [29] S. Fazinić, M. Jakšić, L. Mandić, and J. Dobrinić, *Phys. Rev. A* **74**, 062501 (2006).
- [30] G. Paić and V. Pećar, *Phys. Rev. A* **14**, 2190 (1976).
- [31] R. W. G. Wyckoff, *Crystal Structures* (John Wiley & Sons, New York, 1963).
- [32] S. C. Abrahams, *Phys. Rev.* **130**, 2230 (1963).

- [33] R. Restori, D. Schwarzenbach, and J. R. Schneider, *Acta Crystallogr., Sect. B: Struct. Sci.* **B43**, 251 (1987).
- [34] B. A. Wechsler and R. B. V. Dreele, *Acta Crystallogr., Sect. B: Struct. Sci.* **45**, 542 (1989).
- [35] B. A. Wechsler and C. T. Prewitt, *Am. Mineral.* **69**, 176 (1984).
- [36] B. Song, H. Nakamatsu, R. Sekine, T. Mukoyama, and K. Taniguchi, *J. Phys.: Condens. Matter* **10**, 9443 (1998).
- [37] B. V. Reddy and S. N. Khanna, *Phys. Rev. B* **54**, 2240 (1996).
- [38] X.-B. Wang, D.-C. Tian, and L.-L. Wang, *J. Phys.: Condens. Matter* **6**, 10185 (1994).
- [39] M. Bogovac, I. Bogdanović, S. Fazinić, M. Jakšić, L. Kuček, and W. Wilhelm, *Nucl. Instrum. Methods Phys. Res. B* **89**, 219 (1994).
- [40] M. Jakšić *et al.*, *Nucl. Instrum. Methods Phys. Res. B* **260**, 114 (2007).
- [41] J. Végh, *Nucl. Instrum. Methods Phys. Res. A* **557**, 639 (2006).
- [42] J. Bearden, *Rev. Mod. Phys.* **39**, 78 (1967).
- [43] I. Orlić, J. Makjanić, G. H. J. Tros, and R. D. Vis, *Nucl. Instrum. Methods Phys. Res. B* **49**, 166 (1990).
- [44] J. F. Ziegler, J. P. Biersack, and U. Littmark, *The Stopping and Range of Ions in Solids* (Pergamon Press, New York, 1985).
- [45] M. H. Chen and B. Crasemann, *At. Data Nucl. Data Tables* **41**, 257 (1989).
- [46] J. Wong, F. W. Lytle, R. P. Messmer, and D. H. Maylotte, *Phys. Rev. B* **30**, 5596 (1984).
- [47] F. Gillot, M. Menetrier, E. Bekaert, L. Dupont, M. Morcrette, L. Monconduit, and J. M. Tarascon, *J. Power Sources* **172**, 877 (2007).
- [48] F. Farges, G. E. Brown, and J. J. Rehr, *Phys. Rev. B* **56**, 1809 (1997).
- [49] K. Tsutsumi, O. Aita, and K. Ichikawa, *Phys. Rev. B* **15**, 4638 (1977).
- [50] X. Yang, M. Dubiel, D. Ehrt, and A. Schutz, *J. Non-Cryst. Solids* **354**, 1172 (2008).
- [51] T. Hashimoto, A. Yoshiasa, M. Okube, H. Okudera, and A. Nakatsuka, *AIP Conf. Proc.* **882**, 428 (2007).
- [52] M. Klepka, K. Lawniczak-Jablonska, M. Jablonski, A. Wolska, R. Minikayev, W. Paszkowicz, A. Przepiera, Z. Spolnik, and R. Grieken, *J. Alloys Compd.* **401**, 281 (2005).
- [53] G. A. Waychunas, *Am. Mineral.* **72**, 89 (1987).
- [54] W. B. Kim and J. S. Lee, *J. Catal.* **185**, 307 (1999).
- [55] L. A. Grunes, *Phys. Rev. B* **27**, 2111 (1983).
- [56] A. Balzarotti, M. DeCrescenzi, and L. Incochia, *Phys. Rev. B* **25**, 6349 (1982).
- [57] E. Piskorska, K. Lawniczak-Jablonska, R. Minikayev, A. Wolska, W. Paszkowicz, P. Klimczyk, and E. Benko, *Spectrochim. Acta, Part B* **62**, 461 (2007).
- [58] J. H. Hubbell and S. M. Seltzer, NISTIR Technical Report No. 5632, 1995 (unpublished).
- [59] M. Uršič, M. Kavčič, and M. Budnar, *Nucl. Instrum. Methods Phys. Res. B* **211**, 7 (2003).
- [60] G. Vanko and F. M. F. deGroot, *Phys. Rev. B* **75**, 177101 (2007).
- [61] I. Török, T. Papp, J. Pálinkás, M. Budnar, A. Mühleisen, J. Kawai, and J. L. Campbell, *Nucl. Instrum. Methods Phys. Res. B* **114**, 9 (1996).
- [62] M. Kavčič, M. Budnar, A. Mühleisen, and I. Török, *Nucl. Instrum. Methods Phys. Res. B* **136-138**, 173 (1998).
- [63] V. Ern and A. C. Switendick, *Phys. Rev.* **137**, A1927 (1965).
- [64] D. W. Fischer, *J. Appl. Phys.* **41**, 3922 (1970).
- [65] S. Bartkowski, M. Neumann, E. Z. Kurmaev, V. V. Fedorenko, S. N. Shamin, V. M. Cherkashenko, S. N. Nemnonov, A. Winarski, and D. C. Rubie, *Phys. Rev. B* **56**, 10656 (1997).
- [66] G. Dräger, O. Brümmer, V. Heera, G. Seifert, and P. Ziesche, *Phys. Status Solidi B* **104**, 219 (1981).
- [67] A. S. Koster and H. Mendel, *J. Phys. Chem. Solids* **31**, 2511 (1970).
- [68] D. W. Fischer, *Phys. Rev. B* **5**, 4219 (1972).
- [69] J. A. Tossell, D. J. Vaughan, and K. H. Johnson, *Am. Mineral.* **59**, 319 (1974).
- [70] P. Weinberger, *Theor. Chim. Acta* **42**, 169 (1976).
- [71] M. A. Blokhin and A. T. Shuvaev, *Bull. Acad. Sci. USSR, Phys. Ser. (Engl. Transl.)* **26**, 429 (1962).
- [72] E. E. Vainshtein and V. I. Chirkov, *Sov. Phys. Dokl.* **7**, 724 (1963) [*Dokl. Akad. Nauk SSSR* **145**, 1031 (1962)].